Dovepress

ORIGINAL RESEARCH

Engineered Biomimetic Nanoparticles-Mediated Targeting Delivery of Allicin Against Myocardial Ischemia-Reperfusion Injury by Inhibiting Ferroptosis

Minghui Li[1],*, Jiabi Wu[1],*, Tao Yang[1], Yuhang Zhao[1], Ping Ren[1], Lingling Chang[2], Pilong Shi[1], Jing Yang [1], Yuhang Liu[2], Xiaolei Li[3], Peng Wang[2], Yonggang Cao[1]

[1]Department of Pharmaceutics, Harbin Medical University, Heilongjiang, 163319, People's Republic of China; [2]Department of Physiology, Harbin Medical University, Heilongjiang, 163319, People's Republic of China; [3]Department of Pathology, Jiangsu College of Nursing, Jiangsu, 223003, People's Republic of China

*These authors contributed equally to this work

Correspondence: Peng Wang, Department of Physiology, Harbin Medical University, Xinyang Road 39, Gaoxin District, Daqing, Heilongjiang, People's Republic of China, Email wangpeng810122@126.com; Yonggang Cao, Department of Pharmaceutics, Harbin Medical University, Xinyang Road 39, Gaoxin District, Daqing, Heilongjiang, People's Republic of China, Email caoyonggang@hmudq.edu.cn

Background: Cardiac microvascular damage is substantially related with the onset of myocardial ischaemia-reperfusion (IR) injury. Reportedly, allicin (AL) effectively protects the cardiac microvascular system from IR injury. However, the unsatisfactory therapeutic efficacy of current drugs and insufficient drug delivery to the damaged heart are major concerns. Here, inspired by the natural interaction between neutrophils and inflamed cardiac microvascular endothelial cells (CMECs), a neutrophil membrane-camouflaged nanoparticle for non-invasive active-targeting therapy for IR injury by improving drug delivery to the injured heart is constructed.

Methods: In this study, we engineered mesoporous silica nanoparticles (MSNs) coated with a neutrophil membrane to act as a drug delivery system, encapsulating AL. The potential of the nanoparticles (named AL@MSNs@NM) for specific targeting of infarcted myocardium was assessed using small animal vivo imaging system. The cardiac function of AL@MSNs@NM after treatment was evaluated by Animal Ultrasound Imaging system, HE staining, and Laser Speckle Imaging System. The therapeutic mechanism was analyzed by ELISA kits, immunofluorescence, and PCR.

Results: We discovered that AL@MSNs@NM significantly improves cardiac function index, reduced infarct size and fibrosis, increased vascular perfusion in ischemic areas, and also promoted the function of CMECs, including migration, tube formation, shear stress adaptation, and nitric oxide production. Further research revealed that AL@MSNs@NM have cardio-protective functions in IR rats by inhibiting CMEC ferroptosis and increasing platelet endothelial cell adhesion molecule-1 (PECAM-1) expression.

Conclusion: Our results indicated that AL@MSNs@NM significantly reversed CMEC ferroptosis and increased PECAM-1 expression, enhanced cardiac function, and reduced myocardial infarction size. Therefore, this strategy demonstrates that engineered biomimetic nanotechnology effectively delivers AL for targeted therapy of myocardial infarction.

Keywords: neutrophil membrane, ischemia-reperfusion, allicin, cardiac microvascular endothelial cells, ferroptosis

Introduction

Myocardial infarction is the main cause of fatal heart disease with high morbidity and mortality rates worldwide, triggered by the obstruction of one or more coronary artery blood vessels.[1] The two stages by which myocardial infarction causes myocardial damage are ischaemia and subsequent reperfusion (ischaemia-reperfusion [IR] injury). Reperfusion damage significantly predicts the infarct size and progression to post-infarct heart dysfunction. Recently, increasing blood perfusion at the wounded site has been known to promote recovery following ischaemia. Percutaneous

11275

coronary intervention (PCI) treats myocardial infarction by restoring the blood flow to ischaemic regions.[2] Studies have demonstrated that the new microvasculature can restore cardiac function by compensating for the blood and oxygen supply to the damaged myocardium.[3] Specifically, the incidence of heart failure and death significantly decreased in patients with good collateral circulation following PCI.[4] Therefore, considerable efforts have been made to improve collateral circulation in patients who undergo PCI. Nonetheless, growing evidence suggests that inadequate myocardial reperfusion at the microvascular level is associated with decreased residual left ventricular function, larger infarct size, and increased mortality during follow-up.[5,6] Inhibiting IR injury has become a major focus for treatment because an increased infarct size is associated with reperfusion injury[7] and the great success of treatment in lowering IR.

Early treatment of acute myocardial infarction primarily aims to restore blood flow to the ischaemic risk area, thereby minimising irreversible tissue damage.[8] Although myocardial IR can effectively restore oxygen and blood supply, support cell metabolism, and remove potentially harmful substances from cell metabolism, reperfusion can also cause arrhythmias, diastolic dysfunction, and irreversible metabolic and functional disorders, thereby damaging cardiac function.[9,10] Reportedly, myocardial IR injury comprises three aspects of its mechanism, namely, excessive oxygen free radical production, reperfusion resulting in intracellular calcium overload, and the effect of leukocyte and cardiac microvascular injury.[11–13] Therefore, the primary goal of myocardial infarction treatment is to prevent IR injury. Currently, drug therapy remains one of the primary ways to treat myocardial ischaemic injury.[14] However, the current drug therapy is deficient and has concerns with respect to the drug type, drug duration, and target realisation. Besides, the use of natural products in medicine has gained popularity because of the general perception that they are mild and essentially compared with synthetic chemotherapeutic agents.[15] The primary biologically active component of garlic is allicin,[16] which has purportedly shown to have a variety of biological qualities, including anti-inflammatory, antioxidant, and anti-apoptotic actions, as well as the ability to prevent heart hypertrophy.[17–20] Nonetheless, some studies reveal that allicin is trapped by reactions with fatty acids and proteins in the plasma membrane, limiting its therapeutic effect.[21]

Additionally, the limited target separability and probable toxicity off-target are the main issues with systemic administration of medicines. Poor therapeutic effects are caused by random drug distribution, poor pharmacokinetics, limited bioavailability, quick inactivation, and premature elimination.[22,23] Designing nanomaterials as carriers with controllable size and shape that prevent the degradation of therapeutic agents and control their release in the target tissue could serve as an effective strategy.[24,25]

Currently, engineered cell membrane biomimetic nanotechnology has been widely applied in drug delivery. Cell membranes isolated from natural cells inherit the functions of the original cells and are used to wrap the outer surface of drug-loaded nanoparticles. This approach retains advantages such as prolonged circulation time, efficient and specific targeting, and reduced immune system clearance. Various types of cell membrane-disguised nanoparticles have been developed, including those derived from red blood cells, cancer cells, and immune cells.

Neutrophils (NEs), an important component of the human immune system, can accumulate at sites of inflammation following tissue damage. After acute myocardial infarction, neutrophils are the first to reach the site of inflammation. They then rapidly decompose and form neutrophil extracellular traps (NETs), releasing various signalling factors and recruiting additional immune cells for immune regulation and tissue repair. Nanoparticles disguised with neutrophil membranes can deliver drugs to the heart for the treatment of myocardial infarction. This strategy completely preserves the components of the cell membrane—namely, the complete adhesion molecule system—allowing the biomimetic nanoparticles to exert their function of intercellular communication. Neutrophil membrane biomimetic nanoparticles interact with β2 integrin on neutrophils and ICAM-1 expressed on endothelial cells, adhering to activated endothelial cells and achieving specific targeting.[25]

Herein, we report neutrophil-like nanoparticles with a core-shell structure for the allicin-mediated repair of IR injury. Neutrophils are important immune cells, which on activation, accumulate at inflammatory sites (a phenomenon called chemotaxis), such as the myocardial ischaemic area.[26–28] Hence, location-specific cargo transit is being investigated.[29–32] We investigated whether allicin delivered by nanoparticles to cardiac neutrophils post-IR could be used to target the post-IR inflammation status. Recent studies have reported that allicin could significantly improve the function of CMECs, thereby playing the myocardial protective role,[33,34] which prompted us to adopt the above strategy. Thus, the therapeutic effect of allicin delivered by nanoparticles to the neutrophil-enriched area at the myocardial ischaemic area was

monitored by quantifying the nanoparticle fluorescent signals. The core of mesoporous silica nanoparticles (MSNs) owns a high capacity to load allicin and effectively prevents allicin from reacting with proteins and fatty acids in the plasma membrane. The long-term released allicin at the IR site inhibits ferroptosis of cardiovascular endothelial cells and enhances cardiac microvascular function, thereby protecting the myocardium.

This study constructed neutrophil membrane-coated nanoparticles. By improving drug delivery to damaged hearts, mesoporous core nanoparticles were administered in IR rats to deliver allicin for non-invasive active targeting therapy of IR injury. This approach can effectively inhibit ferroptosis of cardiovascular endothelial cells and improve cardiac microvascular function, thereby protecting the myocardium.

Materials and Methods
Materials
Allicin, oleic acid, cyclohexane, cetyltrimethylammonium bromide (CTAC), 3-aminopropyltriethoxysilane (APTES), and tetraethyl orthosilicate (TEOS) were obtained from Sigma-Aldrich (China). DAPI and fluorescein isothiocyanate (FITC) were purchased from Aladdin (China). DiR was purchased from obtained from HEDE Biotechnology Co. Ltd (Beijing, China). All solvents and reagents used were of analytical standard grade.

Isolation of Neutrophils
Neutrophils were isolated from the peripheral blood of rats using the Percoll gradient method. Blood was drawn into tubes comprising 3.8% sodium citrate, centrifuged to eliminate unwanted components, and finally resuspended in 2 mL of phosphate-buffered saline (PBS). The cell pellets were added to a Percoll gradient solution comprising 78%, 65%, and 55% (volume/volume) PBS. The interface between 65% and 78% was where the neutrophils were identified and retrieved. Using a lysis buffer at 4°C, any remaining erythrocytes were dissolved, allowing for the isolation of highly pure neutrophils, which were then studied under the microscope.

Cell Membrane Derivation
Neutrophil membrane vesicles (NMVs) were extracted in accordance with a previously published protocol. First, the neutrophils were thawed and homogenised. The homogenised solution was centrifuged for 5 min at 3500 rpm and 4°C to eliminate cell nuclei and intact cells. The supernatant was then centrifuged at 4°C for 25 min at 20,000 rpm to separate the mitochondria from the precipitate. The supernatant was centrifuged once again at 4°C and 50,000 rpm for 1 h. After being sonicated for 5 min and extruded 11 times successively through 400 and 100 nm polycarbonate membranes, the NMVs were obtained and stored at −80°C for future use.

Preparation of MSNs
A certain amount cetyltrimethylammonium chloride was combined with deionised water and stirred at 60°C. Then added tetraethyl orthosilicate and cyclohexane and heated the mixture at 60°C for 12 h. The product was cleaned with 0.6% ammonium nitrate ethanol solution thrice. Finally, the MSNs were obtained.

Preparation and Characterization of AL@MSNs@NM
MSNs nanoparticles (5 mg) were dispersed in 5 mL allicin solution (0.2 mg mL^{-1}) for 12 h under magnetic stirring. For membrane camouflaging, NMVs underwent a fusion with an equal volume of MSNs by ultrasound for 5 min, and the resulting specimens were filtered 21 times using porous syringe filters with a membrane pore size of 200 nm. After centrifugation (6000 rpm, 10 min), excess NMVs were removed, and AL@MSNs@NM was obtained.

To prepare FITC labelled MSNs (MSNs-FITC), a certain amount of FITC and APTES were dissolved in anhydrous ethanol by stirring for 24 h, added FITC-APTES at room temperature, and stirring overnight. Finally, the product was washed with deionized water.

Transmission Electron Microscopy (TEM) images and element mapping were captured by transmission electron microscopy (TEM, Tecnai-F30, U.S). N$_2$ adsorption−desorption isotherm was measured on Brunauer-Emmett-Teller

(BET, Micro metrics ASAP, U.S). DLS measurement and Zeta potential were conducted on Nano ZSP (Malvern, UK). Protein analysis was achieved by Western blot analysis.

Myocardial Ischemia-Reperfusion Injury Rat Model

The Wistar male rats (200 ± 20 g) were purchased from the Harbin Medical University Experimental Animal Centre in China. Based on previous descriptions,[35] a rat model of myocardial ischemia-reperfusion (IR) was developed. A left thoracotomy was used to expose the rat's heart, then using a 7–0 silk suture to tie around the left anterior descending coronary artery (LAD) with a slipknot for 45 min of ischemia followed by 6 h of reperfusion.

Cardiac Function Assessment

IR injury was induced as described above, and rats were divided into six groups (n = 6) to determine an appropriate dose of AL@MSNs@NM (allicin: 5, 10, and 20 mgkg^{-1}). AL@MSNs@NM was injected through the tail vein following IR for 14 consecutive days, respectively. For the sham group, rats were subjected to a sham operation and administration of saline in equal amounts. To explore the benefits of different allicin concentrations on cardioprotective effects, echocardiographic assessments were performed to assess cardiac function.

Rats were anesthetized with isoflurane after treatment. According to the previous report,[36] cardiac function was evaluated using echocardiography. Before measurement, the chest region of the rat was shaved, and ultrasound coupling gel was applied to the area. Indicators of cardiac function, including left ventricular ejection fraction (LVEF) and left ventricular fractional shortening (LVFS), were measured utilizing an echocardiographic system with M-mode measurements (Visual Sonics Inc, Canada).

In vivo Imaging

The rats were injected with nanoparticles containing DiR dye via the tail vein immediately after myocardial infarction surgery. The multi-mode function in the Vivo imaging system (Kodak, USA) was used to capture the images to study the nanoparticle distribution with an excitation wavelength of 720 nm and an emission wavelength of 790 nm.

Laser Speckle Contrast Analysis (LSCA) of Infarcted Tissues

After evaluating cardiac function, the MOORFLPI2 real-time blood flow zoom laser speckle imaging system (Moor Instruments, UK) was used to evaluate the flow velocity and spatial vascular contour of the ischemic heart.

Histological Analysis

The hearts were removed from the body and collected in several groupings. Hearts were embedded in an OCT-freeze medium after being fixed in 4% paraformaldehyde, and they were then frozen at −20°C. After that, portions with a 5 μm thickness or less were cut and placed on coated slides. These slices were stained with haematoxylin-eosin and inspected under a light microscope for histological abnormalities. For the evaluation of fibrosis, Masson trichrome staining was performed. Using Image Pro software, the fibrotic region was determined.

Gelatin-Ink Staining

Gelatin-ink staining was used to observe the patency of microvasculature.[37] First, once the IR damage was complete, a gelatin ink (3% gelatin and ink) was injected into the heart through the internal jugular vein at 30°C. The hearts were then harvested and stored at 4°C for 1 h. Finally, after 4% paraformaldehyde fixation, frozen sections were performed, and samples were examined under a microscope.

Primary Rat CMECs Cultures

The CMECs were isolated from the Wistar rats. In brief, we extracted the left ventricle of male rats, followed by the removal of the epicardial coronary artery and endocardial endothelium, following which the remaining tissue was cut into 1 mm^3 segments. Tissue fragments were dissociated by collagen II and then cultured.

Establishment of the Hypoxia Model

In vitro, the hypoxia-reoxygenation (HR) damage model was induced using CMECs. Cells were preconditioned for hypoxia as they were cultivated for 12 h in an incubator. Then, in accordance with other investigations, the CMECs were maintained under normal culture conditions for about 24 h to simulate reperfusion injury.[38]

Western Blot

Hearts were homogenized in a RIPA buffer that contained protease inhibitors, phosphatase inhibitors, and EDTA. The homogenates were centrifuged, and supernatants were extracted and stored at −80°C for further study. The protein was quantified by a BCA protein assay kit. Equal amounts of proteins were separated by SDS-PAGE gels and transferred to polyvinylidene fluoride membranes. After blocking with 5% non-fat milk, membranes were incubated with primary antibodies overnight at 4°C. The secondary horseradish peroxidase-conjugated goat anti-rabbit or anti-mouse IgG antibodies were incubated at room temperature for 1 h. After washing in TBST, the bands were analysed.

Immunofluorescence

To image the expression of PECAM-1, γH2AX, the tissue sections were sequentially processed with 4% paraformaldehyde, permeabilized using 0.2% Triton X-100. Next, sections were incubated overnight with antiPECAM-1 (1:100, Abcam, Cambridge, MA, United States), and antiγH2AX (1:500, Cell Signaling Technology, the United States) at 4∘C. Then, the tissues were incubated with secondary antibody for 1 h at room temperature and the tissues were counterstained with DAPI (Beyotime Biotechnology, Shanghai, China) for the identification of nuclei. The samples were observed and photographed under a microscope.

Nitrite Detection

The levels of NO are measured by testing the levels of nitrate and nitrite in the samples. This process utilizes the Griess Reaction Nitric Oxide Assay Kit (Calbiochem, San Diego, CA, United States). The amount of NO in the samples is determined and normalized to the total protein content of the samples, with results expressed in picomoles per milligram of protein (pmol/mg protein).

Real-Time qPCR

Total RNA was extracted from cardiac tissues using TRIZOL reagent (Invitrogen, Carlsbad, CA, USA). Gene expression was quantified using a NanoDrop-2000 spectrophotometer (Thermo Fisher Scientific, Waltham, MA, USA). Complementary DNA (cDNA) was synthesized with reverse transcriptase (AR121-mix, Innovagene, Hunan, China). Real-time PCR was then conducted using a Real-Time System (Analytik Jena, Germany) with SYBR Green qPCR Mix (SQ121-01, Innovagene, Hunan, China). The $2-\Delta\Delta Ct$ method was used for data analysis, and results were normalized and expressed as relative mRNA levels.

Statistical Analysis

The data was displayed as mean SD. With Origin 9.0, statistical analyses were carried out. The two-tailed unpaired Student's *t*-test was used to compare any two groups. One-way analysis of variance procedures was used to compare data from more than two groups. Differences in statistics outcome analysis were deemed statistically significant when P 0.05.

Results and Discussion

Synthesis and Characterisation of AL@MSNs@NM

As illustrated in Scheme 1, we prepared AL@MSNs@NM delivery system by a top-down approach reported previously for treating the myocardial IR injury. Firstly, to prepare the NMVs, we successfully isolated the neutrophils (Figure 1A). Then, the neutrophil membrane was extracted according to the published protocol with fit modifications and extruded through a polycarbonate membrane (200 nm). The obtained NMVs were mixed with drug-loaded MSNs to obtain AL@MSNs@NM. The TEM and SEM images in Figure 1B reveal that MSNs exhibited a uniform, well-dispersed sphere
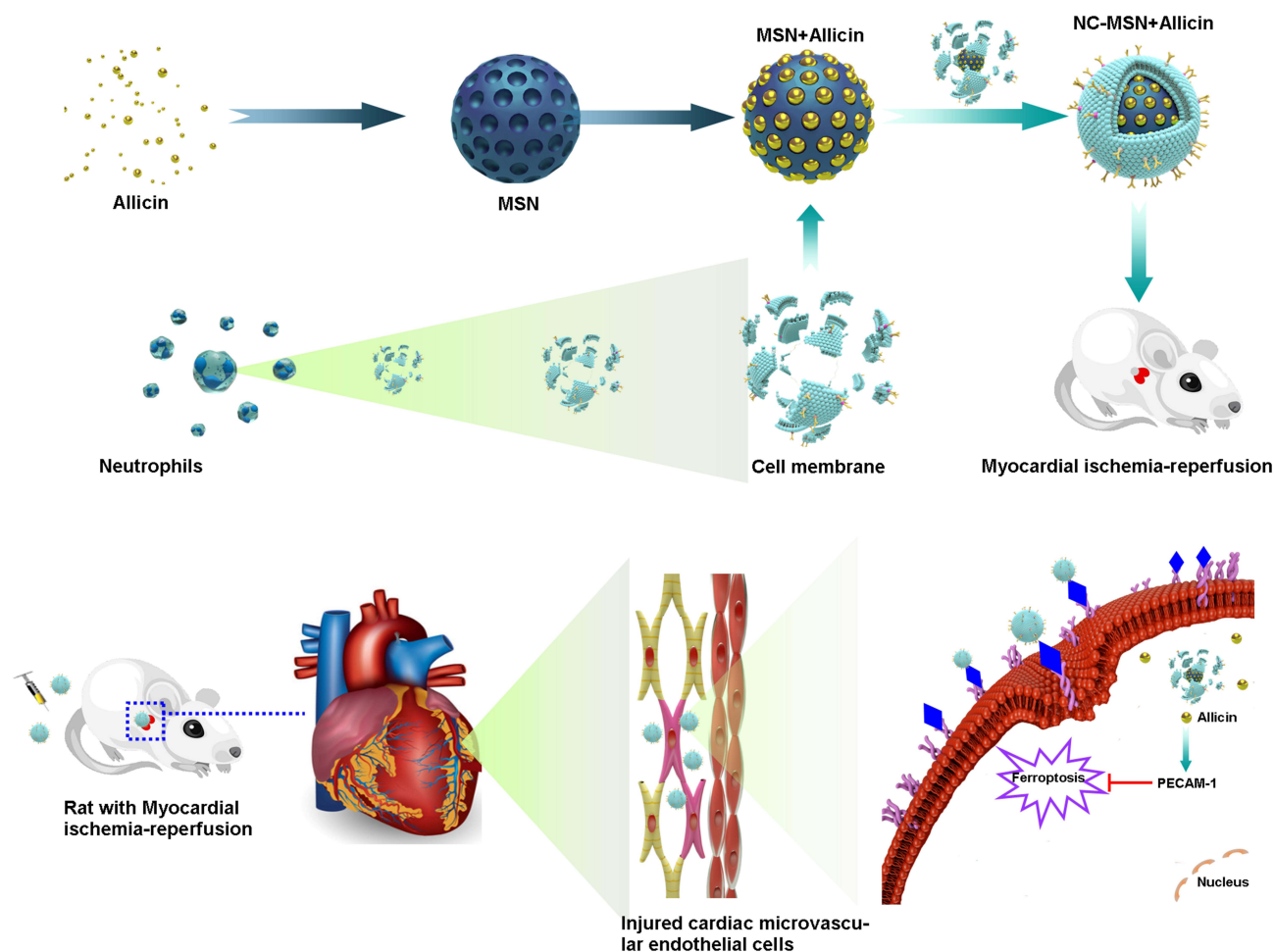
Scheme 1 Neutrophil cell membrane-camouflaged nanoparticles for the allicin-mediated repair of ischaemia-reperfusion injury. Schematic illustration of the fabrication of neutrophil membrane-camouflaged mesoporous silica nanoparticles with allicin AL@MSNs@NM. AL@MSNs@NM targets ischaemic myocardium. Upon the uptake by cardiac microvascular endothelial cells (CMECs), AL@MSNs@NM decomposes in CMECs and releases allicin into the cytoplasm. Allicin promotes PECAM-1 protein expression to inhibit CMECs ferroptosis.

with an average size of approximately 90 nm. On coating the NMVs, AL@MSNs@NM were stained with 2% phosphotungstic acid and visualised using TEM. As displayed, AL@MSNs@NM showed a "eukaryotic cell"-like structure with an outermost layer that was light grey and had a thickness of around 10 nm, which was commensurate with the thickness of the cell membrane, indicating a successful membrane camouflaging on the MSNs@NM. Additionally, the elemental mapping pictures showed where silicon, oxygen, and tungsten were distributed in MSNs@NM nanoparticles (Figure 1C). The MSNs core was distributed with silicon and oxygen, and the cell membrane with tungsten. The X-ray diffraction pattern showed that the MSNs had a broad diffraction peak of about 22° at 2θ rather than any obvious peak (Figure 1D). The surface of the MSNs had a well-aligned mesoporous structure with a diameter of around 2.3 nm, 0.89 mL g^{-1} of pore volume, and 498 m^2 g^{-1} of surface area (Figure 1E), which could subsequently help in allicin loading. The loading efficiency of AL in MSNs was ~8%. To determine the stability in solution over time, AL@MSNs@NM were stored in PBS or FBS (1%) at 4°C and they exhibited stable size with only a slight increase in particle size within 7 days (Figure 1F). To verify the safety of AL@MSNs@NM, a hemolysis assay was conducted using Red Blood Cells (RBCs). As shown in Figure 1G, no significant hemolysis occurred when various doses of AL@MSNs@NM were added. The absorbance of the supernatant from the blood samples was measured at 540 nm. The results indicate that even at a concentration of 100 μg/mL, the hemolysis rate remained low—less than 5%. Due to lymphocyte function-associated antigen (LFA-1) and β2 integrin were present, MSNs@NM could be effectively targeted to the wounded CMECs. WB was further used to confirm the presence of the cell membrane proteins β2 integrin and
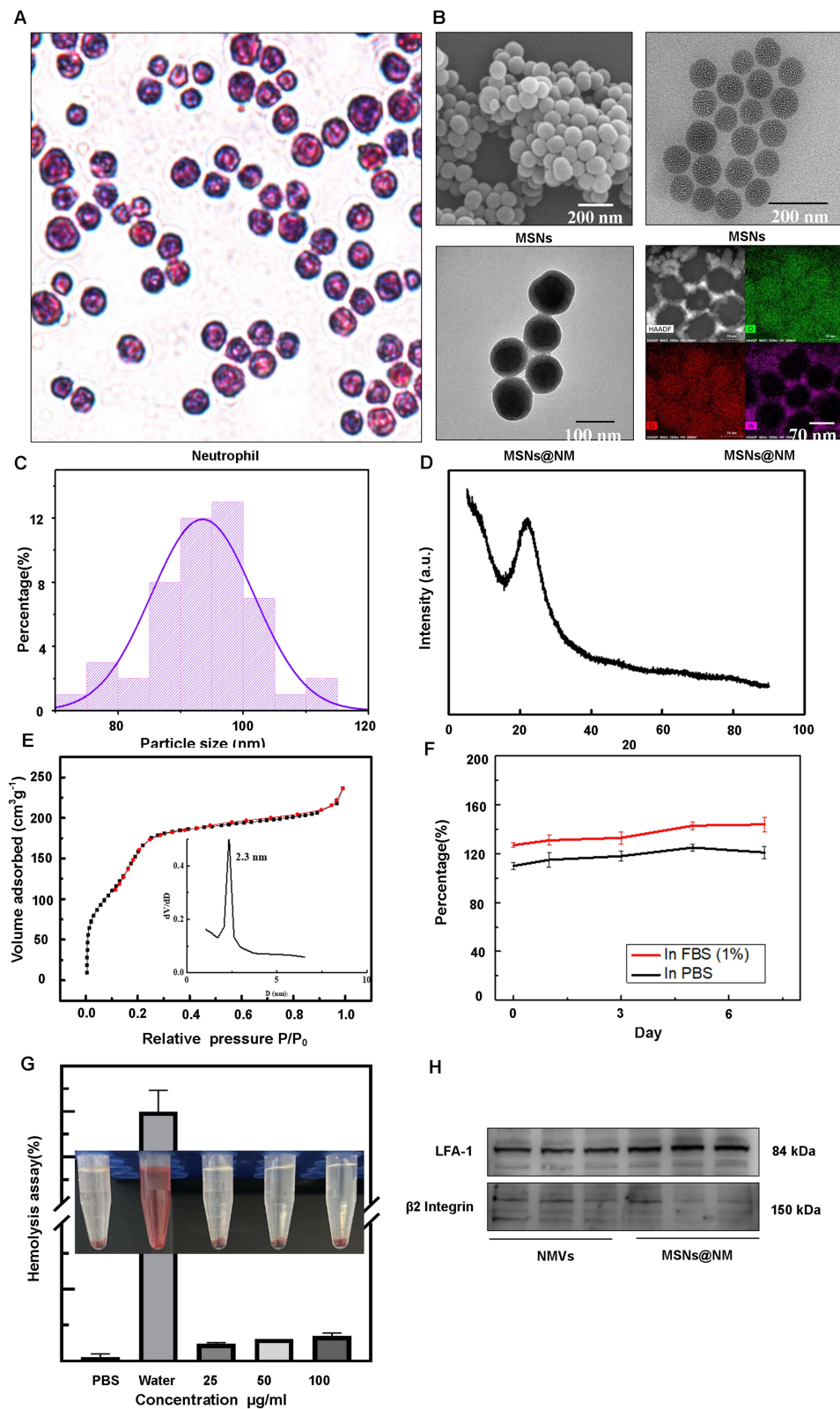
Figure 1 Characterization of the nanoparticles. (**A**)The representative microphotographs of neutrophils stained with haematoxylin and eosin (×400). (**B**) Scanning electron microscopy images of mesoporous silica nanoparticles (MSNs), Transmission electron microscopy images of MSNs, Neutrophil membrane-camouflaged (NM) mesoporous silica nanoparticles (MSNs@NM) and Elemental mapping of MSNs@NM. (**C**)Diameter distribution of MSNs. (**D**) X-ray diffraction analysis of MSNs. (**E**) Nitrogen adsorption-desorption isotherms analysis of MSNs. (**F**)The hydrate particle size of AL@MSNs@NM in PBS and FBS (1%) as a function of time. (**G**) Hemolysis assays. The photos illustrating the hemolysis effects of RBCs after 8 h incubation with AL@MSNs@NM in different concentrations. PBS and water were set as negative (-) and positive (+) controls, respectively. (**H**) Western blotting analysis of NMVs proteins including LAF-1 and β_2 integrin from NMVs and MSNs@NM.

LFA-1 on MSNs@NM. As expected, the LFA-1 and β_2 integrin bands of MSNs@NM were similar to that of the NMVs on sodium dodecyl sulphate-polyacrylamide gel electrophoresis. MSNs@NM did not lose much protein in the preparation process. (Figure 1H).

The Cellular Tropism of MSNs@NM in vivo

To explore the tropism capability of MSNs@NM to injured CMECs, CMECs were pretreated with hypoxia reoxygenation (H/R) and then treated with MSNs and MSNs@NM. CMECs under H/R with PBS were used as control groups. Fluorescence images exhibited that the amount of MSNs@NM binding to CMECs was highest in contrast to MSNs or PBS under hypoxia. However, the binding number of MSNs and MSNs@NM was statistically different, implying that MSNs modified neutrophils membrane carriers mainly bind to injured CMECs (Figure 2A).

The cellular uptake of MSNs@NM was measured using Flow cytometry analysis, as shown in Figure 2B and C. The fluorescence intensity of MSNs@NM was significantly higher than that of PBS and MSNs groups. These finding also indicated that we successfully developed MSNs@NM delivery nanocarriers, thereby exerting a more effective therapeutic effect.

Screening Optimal Dose and Targeting Biodistribution in vivo

We firstly established an ischemia-reperfusion rat model. In detail, the temporary left anterior descending coronary artery closure for 45 min was followed by a 6 h reperfusion to create the rat model of IR. The successful establishment of the model was confirmed by the ST-segment elevation on the electrocardiogram, and in the AL@MSNs@NM group, the ST-segment elevation was alleviated (Figure S1).

In addition, a significant increase in Ly6G positive neutrophils was confirmed by immunofluorescence assay in the IR rat (Figure S2). The treatment regimen was shown in Figure 3A. To determine the optimal injection dose of AL@MSNs@NM in vivo, the rats with IR injury were randomly divided into six groups, and effective doses were screened. The representative cardiac function indices were assessed. Left ventricular ejection fraction (LVEF) values in the sham, saline, MSNs@NM, AL@MSNs@NM-5, AL@MSNs@NM-10, and AL@MSNs@NM-20 groups (allicin: 5, 10, and 20 mg kg^{-1}) were 67.3%, 28.3%, 30.2%, 29.8%, 60.2%, and 61.3%, respectively. The left ventricular fractional shortening (LVFS) values in the sham, saline, MSNs@NM, AL@MSNs@NM-5, AL@MSNs@NM-10, and AL@MSNs@NM-20 groups were 37.8%, 17.2%, 16.9%, 17.8%, 31.4%, and 33.1%, respectively. In comparison with the other groups, the AL@MSNs@NM-10 and AL@MSNs@NM-20 groups demonstrated better restoration of the LVEF and LVFS (Figure 3B–D), exhibiting the remarkable therapeutic efficiency of AL@MSNs@NM-10 and AL@MSNs@NM-20 in improving the injured cardiac function. Therefore, for safety reasons, we finally used a single injection (10 mg kg^{-1}) for the following in vivo experiment.

Subsequently, ex vivo fluorescence imaging was used to demonstrate the infarct-heart homing ability of DIR@MSNs@NM in vivo. The ischemia-reperfusion rats with IR injury were intravenously injected with free DiR, DIR@MSNs, and DIR@MSNs @NM. As a control, the Sham-operated rat was administered DIR@MSNs@NM(Sham). Then, the rats were anesthetized, and their hearts and other organs were isolated. As shown in Figure 3E, a faint fluorescent signal was seen in the heart of the DIR@MSNs group. However, in the DIR@MSNs@NM group, a considerable signal was observed in the heart, indicating that DIR@MSNs@NM specifically heart homing ability. In other organs, no significant fluorescent signal, such as the spleen, lungs, and kidneys, exhibited a significantly lower distribution of DIR@MSNs@NM (Figure 3F).

Reduce Myocardium Damage by AL@MSNs@NM in vivo

Based on the above results, AL@MSNs@NM could effectively accumulate in the damaged heart and significantly improve heart function. Next, we further verified whether AL@MSNs@NM had a therapeutic effect in rats with IR. The IR rats were randomly divided into four groups, each receiving intravenous injection of saline and AL, AL@MSNs, and AL@MSNs@NM. As a control, the Sham-operated rat was administered saline (Sham). After treatment, evaluate the recovery of blood flow and evaluate the flow velocity and spatial vascular contour of the infarcted heart through LSCA. As shown in Figure 4A, compared to the sham group, the blood flow was severely obstructed for IR hearts with saline.
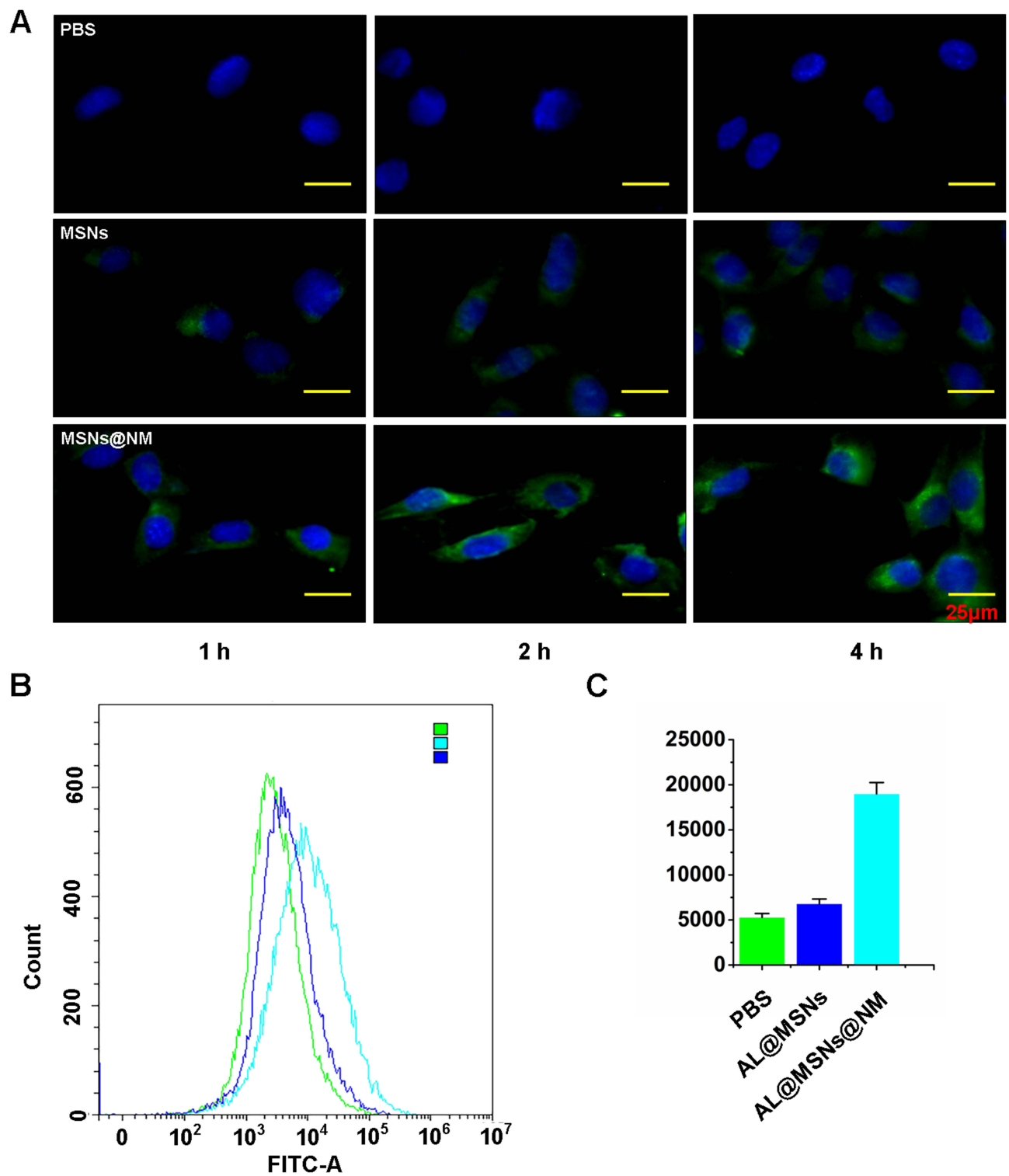
Figure 2 Targeting ability of nanoparticles in vitro. (**A**)Fluorescence images showing intracellular localization MSNs and MSNs@NMinCMECs after H/R treatment. The nanoparticles and nuclei were stained with MSNs-FITC (green) and DAPI (blue), respectively. (**B**) Flow cytometry analysis of cellular uptake of MSNs and MSNs@NM by CMECs(**C**) the quantitative assay.

AL and AL@MSNs group were not significantly affect on blood flow reconstruction. AL@MSNs@NM group could enhance blood flow, and the results were more pronounced.

The infarct size was a key parameter of cardiac function. Therefore, after treatment with different groups, the isolated hearts were stained with triphenyl tetrazolium chloride to determine the infarct area. As shown in Figure 4B and C, the
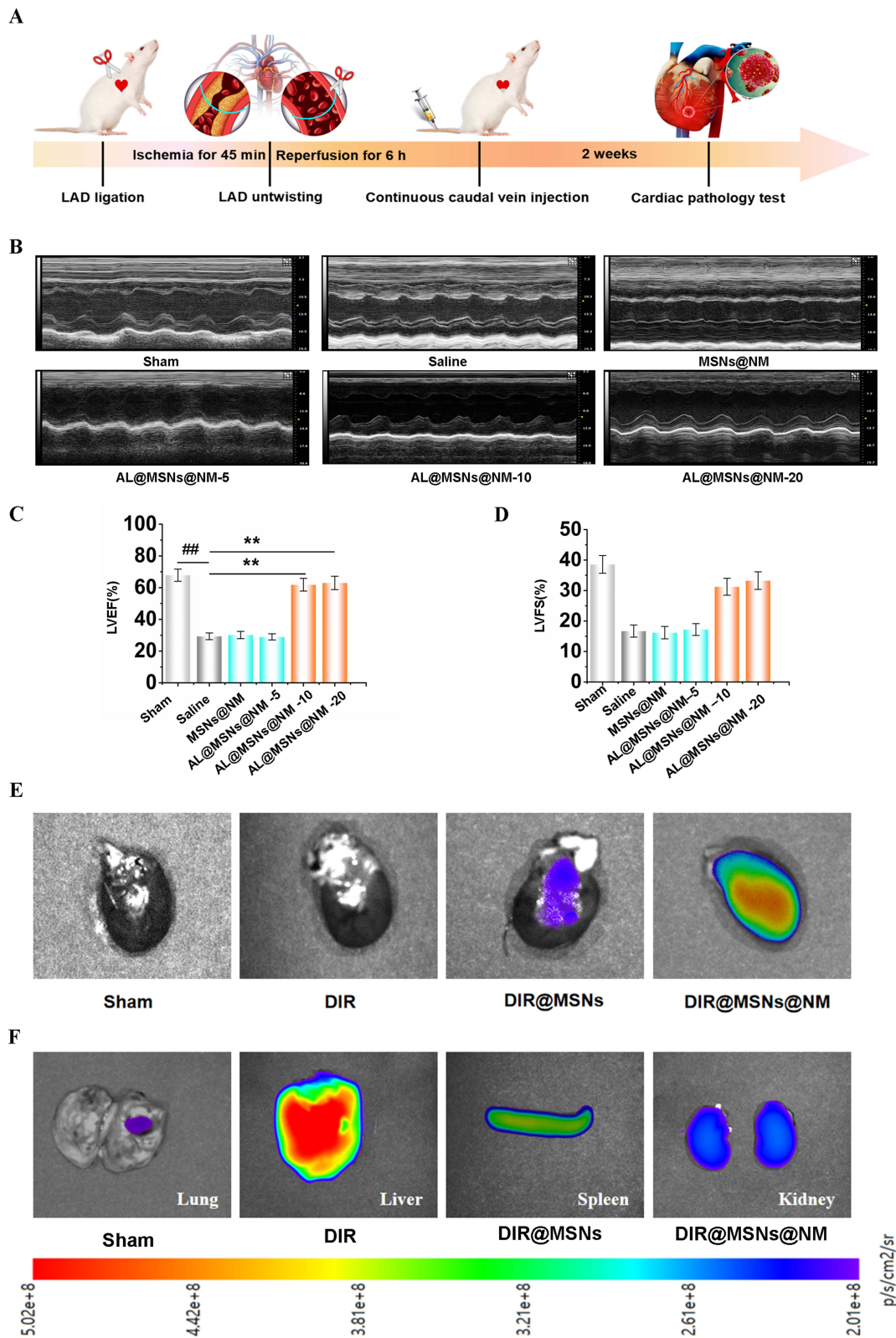
Figure 3 Local AL delivery improves cardiac function and Targeting distribution ability. (**A**)Time line for the design of the animal study. (**B**) Representative M-mode images analysis to assess cardiac function, the IR hearts treated with saline, MSNs@NM, AL@MSNs@NM-5, AL@MSNs@NM-10, and AL@MSNs@NM-20, severally. (**C**) left ventricle ejection fraction (LVEF), (**D**) left ventricle fractional shortening (LVFS).(**E**)Bio-distribution fluorescent images of individualized groups in isolated heart.(**F**) Fluorescence distribution images of isolated organs treated with DIR@MSNs@NM(lung, liver, spleen, kidney). The data are expressed as the mean ± SEM. $^{\#\#}P < 0.01$ compared to Sham group, $^{**}P < 0.01$ compared to Saline group.
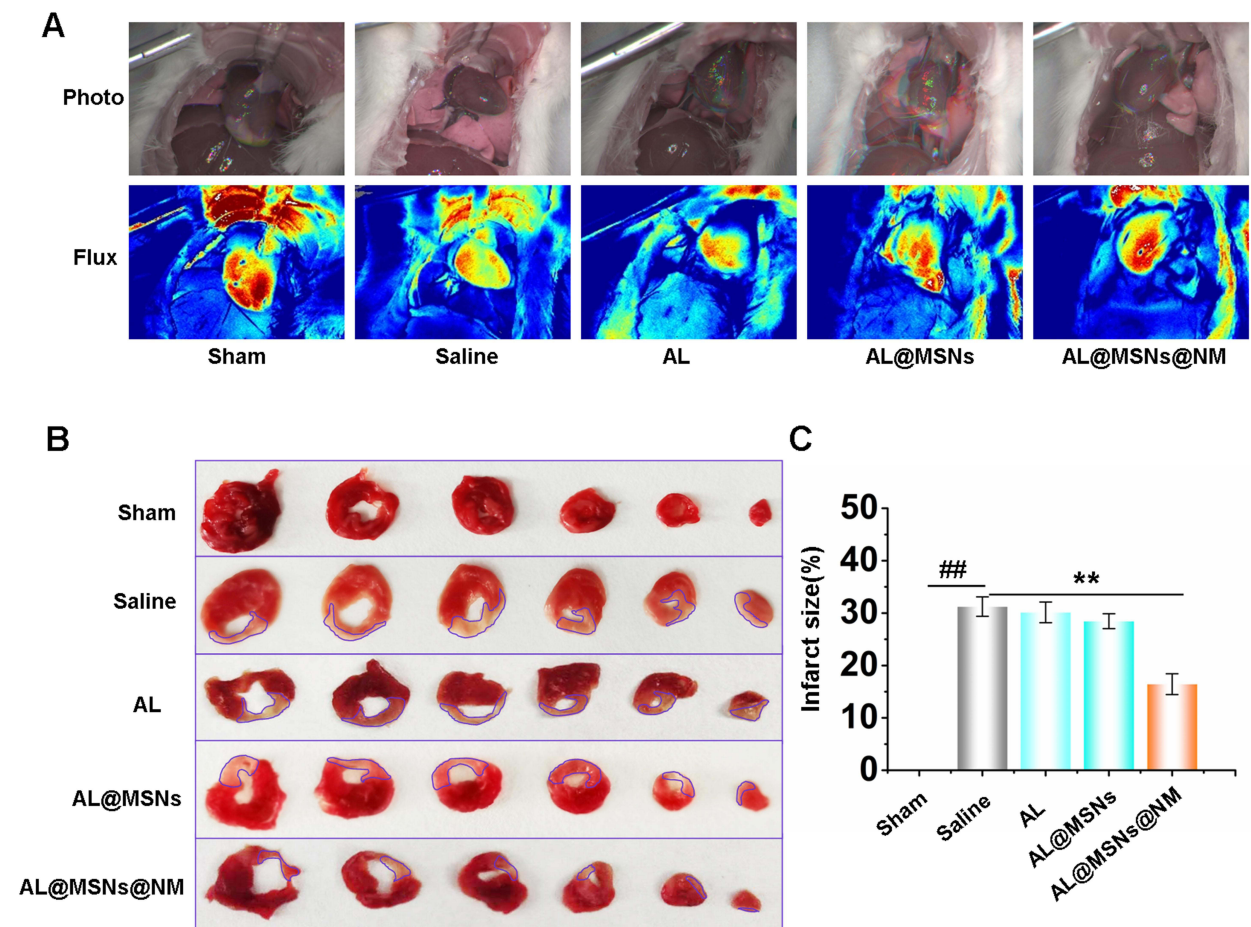
Figure 4 Results of Blood flow restoration and infarct size. (**A**) Photos and flux heat map in the heart of various groups were evaluated by LSCA. The images are representative image of groups of the sham, saline, AL, AL@MSNs, and AL@MSNs@NM with a magnet, respectively. (**B**) Representative illustrations of the infarct size, as determined by triphenyl tetrazolium chloride (TTC) staining. (**C**)Myocardial infarction area statistical chart. The data are expressed as the mean ± SEM.$^{\#\#}P < 0.01$ vs Sham group; $^{**}P < 0.01$ vs Saline group.

infarcted areas in the sham, saline, AL, AL@MSNs, and AL@MSNs@NM groups accounted for 0.01%, 31.4%, 30.7%, 27.4%, and 16.8%, respectively. The AL@MSNs@NM groups demonstrated smaller infarcted areas compared to the other group. The findings also consisted with the results above and suggested that AL@MSNs@NM could enhance the blood flow recovery and reduce myocardial infarction size.

Subsequently, haematoxylin and eosin staining was performed to observe the pathological structure of the myocardial tissue. In the sham group, the myocardium was complete, the muscle fibres were arranged neatly, and no inflammatory cell infiltration was observed. In the saline group, the cardiomyocyte was disorderly arranged, with a large number of infarcted foci, cytoplasmic swelling, significant myolysis, and a large amount of neutrophil infiltration in the stroma. However, AL@MSNs@NM treatment significantly improved the disorderly arrangement of the myocardial cells and effectively reduced the severity of myocardial infarction (Figure 5A). To further study myocardial fibrosis, heart tissue sections were stained with Masson's trichrome. The sham group showed no overt myocardial fibrosis, but the saline, AL, and AL@MSNs groups showed considerable myocardial fibrosis. In addition, minimal myocardial fibrosis was observed in the AL@MSNs@NM group, which benefited from the highly efficient targeting of AL@MSNs@NM (Figure 5B).

Concurrently, γH2AX was a marker of DNA double-stranded breaks and can therefore be used to monitor DNA repair. The immunofluorescence revealed that γH2AX expression increased in saline, AL, and AL@MSNs groups, however, the AL@MSNs@NM group significantly decreased (Figure 5C).
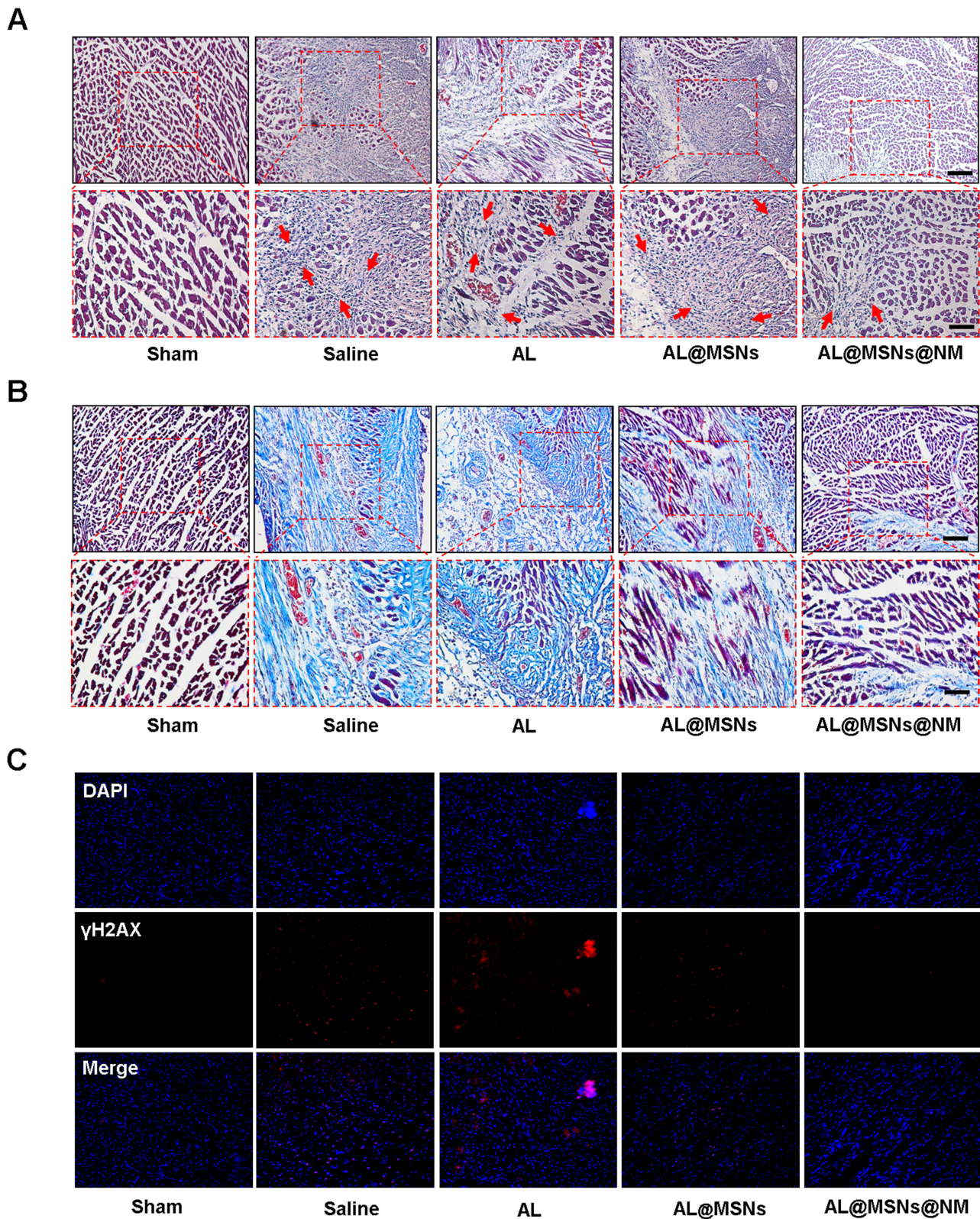
Figure 5 (**A**) Representative images of haematoxylin and eosin-stained heart sections of the ischaemia-reperfusion hearts treated with phosphate-buffered saline (PBS), allicin (AL), mesoporous silica nanoparticles with allicin (AL@MSNs), and neutrophil membrane-camouflaged mesoporous silica nanoparticles with allicin (AL@MSNs@NM). (**B**) Representative images of Masson's trichrome-stained heart sections of the ischaemia-reperfusion hearts treated with PBS, AL, AL@MSNs, and AL@MSNs@NM. (**C**) Distribution of γH2AX was assessed by immunofluorescence (red), and cell nuclei were identified using DAPI (blue).

## Improvement in the Microvascular Function by AL@MSNs@NM

To assess the protective effect of microvascular damage of AL@MSNs@NM in vivo, the cardiac micro-vessel density of the ischemic areas of IR hearts was examined. As shown in Figure 6A, Gelatine-ink staining revealed that the saline group had very low levels of cardiac micro-vessel density. The cardiac micro-vessel density revealed a negligible change in the AL and AL@MSNs groups, while that in the AL@MSNs@NM group increased significantly. Then, we observed the expression of PECAM-1 by immunofluorescence. As shown in Figure 6B, compared with the sham group, the fluorescence density was significantly reduced in the saline group, while that in the AL@MSNs@NM group increased significantly. These results indicated that AL@MSNs@NM had a protective effect on cardiac microvascular injury in IR rats.

The cardiac micro-vessel function was further assessed by the content of nitric oxide. The data revealed that the nitric oxide content significantly decreased in the saline group, however, AL@MSNs@NM group increased the nitric oxide content (Figure 6C). Recent studies had reported that myocardial IR injury was associated with ferroptosis. The ubiquitin-specific peptidase 22 is protected against myocardial IR injury via the sirtuin 1-p53/solute carrier family 7 member 11-dependent inhibition of ferroptosis-induced cardiomyocyte death.[39] During IR injury, oxidized phosphatidylcholines cause ferroptosis in cardiomyocytes.[40] Therefore, we identified the effect of AL, AL@MSNs, and AL@MSNs@NM on ferroptosis in myocardial tissue. Superoxide dismutase (SOD), manganese SOD, copper/zinc-SOD, plasma glutathione peroxidase, catalase, glutathione, and malondialdehyde were all evaluated as oxidative stress indicators. According to our findings (Figure S3A–G), only AL@MSNs@NM prevented oxidative stress in the hearts of IR rats. Importantly, AL@MSNs@NM significantly reduced prostaglandin-endoperoxide synthase 2 (ptgs2) messenger RNA (mRNA) expression, a ferroptotic marker[41] (Figure 6D). These results indicated that AL@MSNs@NM could target areas of myocardial IR injury and exert a protective effect by inhibiting ferroptosis.

AL@MSNs@NM Inhibited CMEC Ferroptosis by Targeting PECAM-1

A H/R model of CMECs was established following temporary hypoxia for 12 h, followed by a 24 h reperfusion to evaluate the therapeutic effect of AL@MSNs@NM in vitro. The scheme of the timeline revealed the design of the cell study (Figure 7A). Cellular treated with AL@MSNs@NM for 48 h, followed by an evaluation of the shear adaptation, tube formation, and migratory functions of CMECs. Before cell function experiments, the cell viability of AL@MSNs@NM in different concentrations was analyzed after treatment with CCK-8 analysis. The CMEC cells after H/R treatment were incubated with 25, 50, and 100 μM of AL in AL@MSNs@NM. The untreated cells served as the control. As shown in Figure 7B, AL@MSNs@NM groups (50 and 100 μM) had considerably higher cell viability than the control group.

To assess the PECAM-1 expression, immunofluorescence was also performed. As shown in Figure 7C, H/R-treated CMECs drastically lacked PECAM-1. On the other hand, AL@MSNs@NM (50 μM) markedly elevated the PECAM-1 expression. We further evaluated the effects of AL@MSNs@NM (50 μM) on CMEC migration by cell scratching. As shown in Figure 7D, AL@MSNs@NM (50 μM) significantly improved cell migration. Additionally, CMEC tubular function experiment also confirmed that AL@MSNs@NM had a protective effect on myocardial hypertrophy via enhancing cardiac microvascular function. As shown in Figure 7E, after H/R therapy, we noticed that tube formation decreased, however, AL@MSNs@NM reversed this impact. A suitable shear stress value was essential for cell survival because endothelial cells respond to variations in local shear stress by changing their rates of proliferation, apoptosis, differentiation, and migration.[42] Therefore, we verified whether AL@MSNs@NM could restore the adaptability of endothelial cells after H/R-induced. The findings showed that the control cells responded to shear stress promptly, elongating $66.31 \pm 5.0\%$ of the cells after 24 h. Only $35.6 \pm 3.6\%$ of the cells in H/R-treated cells underwent elongation after the first 24 h, whereas $46.2 \pm 4.3\%$ of the cells in AL@MSNs@NM group underwent elongation after 24 h, with the role of AL@MSNs@NM becoming redundant after being silenced by PECAM-1. Upon reaching full shear adaptation after 72 h, both the control and AL@MSNs@NM group underwent elongation of more than 75%. Comparatively, only $53.2 \pm 4.1\%$ of the silencing PECAM-1-treated cells and $52.7 \pm 3.5\%$ of the H/R-treated cells exhibited elongation at 72 h. Until 120 h after shear onset, all groups reached full shear adaptation. Taken together, there existed a delay in shear adaptation in H/R-treated CMECs, and AL@MSNs@NM could improve the adaptive capacity for the shear stress of CMECs (Figure 7F and G). Following H/R treatment, the nitric oxide concentration reduced, but H/R's effects were
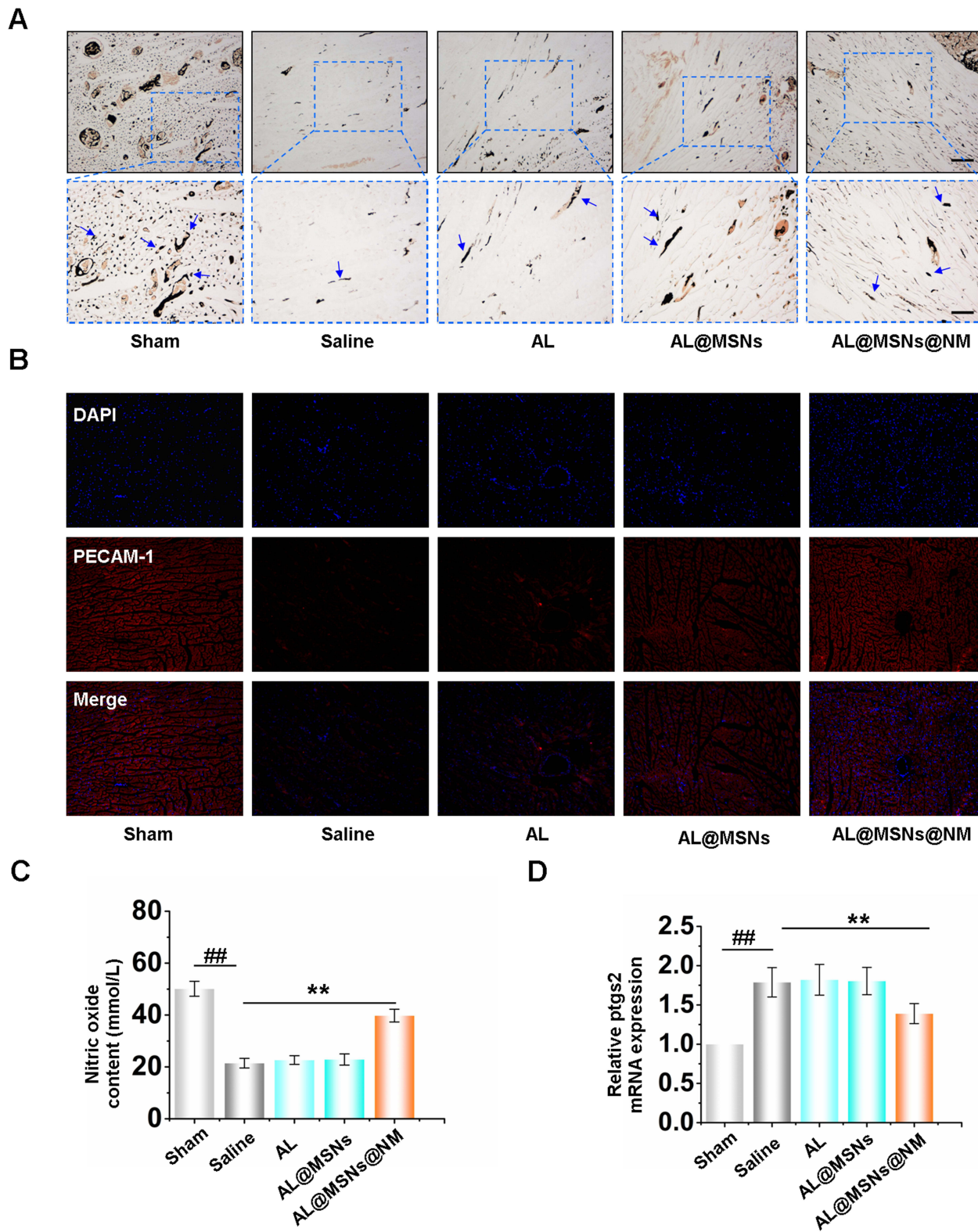
Figure 6 (**A**) Representative image of gelatine-ink staining. Scale bars, up panel is 200 μm (×100); down panel is 100 μm (×200). (**B**) Distribution of PECAM-1 was assessed by immunofluorescence (red), and cell nuclei were identified using DAPI (blue). (**C**) Statistical analysis chart of the nitric oxide content. (**D**) The mRNA expression of ptgs2 in CMECs. The data are expressed as the mean ± SEM. ##$P < 0.01$ vs Sham group; **$P < 0.01$ vs Saline group.
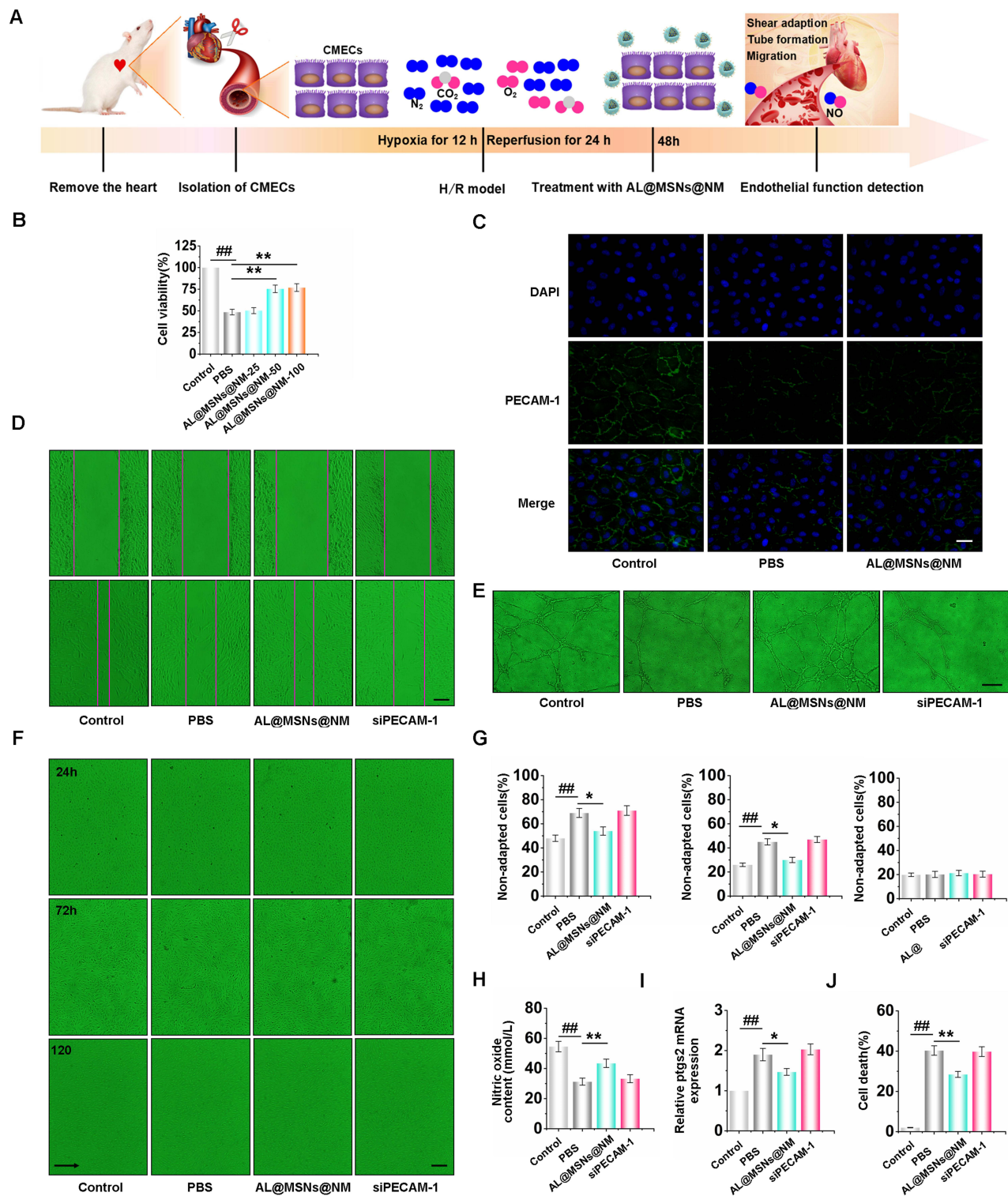
Figure 7 Improved the function of CMECs by up-regulating PECAM-1. (**A**)Timeline for the design of cell study. (**B**) The effects of AL@MSNs@NM on cell viabilities of hypoxia (**H**)/reoxygenation ®-treated CMECs. (**C**) The effects of AL@MSNs@NM on the distribution of PECAM-1 of CMECs treated by H/R.(**D**) Representative images of CMECs migrating after AL@MSNs@NM treatment for 24 h. (**E**). Representative images of CMEC tube formation in three-dimensional collagen gels after AL@MSNs@NM treatment for 8 h. (**F, G**) Effects of AL@MSNs@NM on the shear adaptation of H/R-treated cells. Statistical analysis for the non-adapted cells at 24, 72, and 120 h.(**H**) Statistical analysis chart of the nitric oxide content. (**I**) The messenger ribonucleic acid expression of prostaglandin-endoperoxide synthase 2 in CMECs. (**J**) Statistical analysis of CMEC ferroptosis. The data are expressed as the mean ± SEM. $^{\#\#}P < 0.01$ vs Control group; $*P < 0.05$, $**P < 0.01$ vs PBS group.

restored by AL@MSNs@NM (Figure 7H). Furthermore, to identify the effects of AL@MSNs@NM on H/R-induced CMEC ferroptosis, we analysed the ptgs2 mRNA level. Our results revealed that the ptgs2 mRNA level significantly decreased in the AL@MSNs@NM treatment groups than those of the PBS group, while the protective effect of AL@MSNs@NM disappeared after being silenced by PECAM-1 (Figure 7I). The cell death statistical analysis revealed that AL@MSNs@NM significantly inhibited H/R-induced CMEC death (Figure 7J). These data suggested that AL@MSNs@NM inhibited CMEC ferroptosis by targeting PECAM-1 (Supplementary Material).

Conclusions

Herein, we successfully established a novel biomimetic nanoplatform based on membrane-coated neutrophil-MSNs for delivering allicin to repair IR injury. AL@MSNs significantly accumulated the infarcted myocardium and alleviated oxidative stress induced by H/R, resulting in better therapeutic outcomes. Based on these findings, the modification of endothelial migration, tube formation, shear stress adaptation, and nitric oxide production via allicin supplementation should be considered an effective approach for inhibiting IR injury. Moreover, our results indicated that AL@MSNs@NM significantly reversed CMEC ferroptosis and increased PECAM-1 expression. Therefore, neutrophil biomimetic-targeted CMECs might be a preferable platform to clinically introduce heart reparative procedures.

Therefore, neutrophil biomimetic nanoparticles targeting cardiac microvascular endothelial cells (CMECs) may serve as the preferred platform for cardiac drug delivery. This strategy provides a solid foundation for improving cardiac function in the treatment of myocardial infarction and explores the potential of using biomimetic drug delivery systems to treat other cardiovascular diseases.

Ethical Approval Statement

All experiments were conducted in accordance with the National Institutes of Health Guidelines for the Care and Use of Experimental Animals (NIH Publication No. 8023, revised 1978) and approved by the Experimental Animal Ethics Committee of Harbin Medical University, China (Animal Experimental Ethical Inspection Protocol NO. HMUDQ20230128001). All rats were purchased from the Harbin Medical University Experimental Animal Centre in China, housed in a specific pathogen-free environment (ventilated room, 24±2°C, 55–65% humidity), and had free access to standard water and food.

Acknowledgments

Disclosure

The authors declare that they have no known competing financial interests or personal relationships that could have appeared to influence the work reported in this paper.

References

1. Groehler A, Kren S, Li Q, et al. Oxidative cross-linking of proteins to DNA following ischemia-reperfusion injury. *Free Radic Biol Med*. 2018;120:89–101. doi:10.1016/j.freeradbiomed.2018.03.010
2. Heusch G, Gersh BJ. The pathophysiology of acute myocardial infarction and strategies of protection beyond reperfusion: a continual challenge. *Eur Heart J*. 2017;38(11):774–784. doi:10.1093/eurheartj/ehw224
3. Quan Z, Wang QL, Zhou P, Wang GD, Tan YZ, Wang HJ. Thymosin β4 promotes the survival and angiogenesis of transplanted endothelial progenitor cells in the infarcted myocardium. *Int J Mol Med*. 2017;39(6):1347–1356. doi:10.3892/ijmm.2017.2950
4. Ferrante G, Belli G, Presbitero P. Letter by Ferrante et al regarding article, "impact of collateral flow to the occluded infarct-related artery on clinical outcomes in patients with recent myocardial infarction: a report from the randomized occluded artery trial". *Circulation*. 2011;123(8):e256. doi:10.1161/circulationaha.110.977645 author reply e257-8.
5. Nijveldt R, Beek AM, Hirsch A, et al. Functional recovery after acute myocardial infarction: comparison between angiography, electrocardiography, and cardiovascular magnetic resonance measures of microvascular injury. *J Am Coll Cardiol*. 2008;52(3):181–189. doi:10.1016/j.jacc.2008.04.006
6. Bax M, de Winter RJ, Schotborgh CE, et al. Short- and long-term recovery of left ventricular function predicted at the time of primary percutaneous coronary intervention in anterior myocardial infarction. *J Am Coll Cardiol*. 2004;43(4):534–541. doi:10.1016/j.jacc.2003.08.055

7. Larose E, Rodés-Cabau J, Pibarot P, et al. Predicting late myocardial recovery and outcomes in the early hours of ST-segment elevation myocardial infarction traditional measures compared with microvascular obstruction, salvaged myocardium, and necrosis characteristics by cardiovascular magnetic resonance. *J Am Coll Cardiol*. 2010;55(22):2459–2469. doi:10.1016/j.jacc.2010.02.033

8. Cadenas S. ROS and redox signaling in myocardial ischemia-reperfusion injury and cardioprotection. *Free Radic Biol Med*. 2018;117:76–89. doi:10.1016/j.freeradbiomed.2018.01.024

9. Johnson AP, Parlow JL, Whitehead M, Xu J, Rohland S, Milne B. Body mass index, outcomes, and mortality following cardiac surgery in Ontario, Canada. *J Am Heart Assoc*. 2015;4(7). doi:10.1161/jaha.115.002140

10. Kang B, Li W, Xi W, et al. Hydrogen sulfide protects cardiomyocytes against apoptosis in ischemia/reperfusion through MiR-1-regulated histone deacetylase 4 pathway. *Cell Physiol Biochem*. 2017;41(1):10–21. doi:10.1159/000455816

11. Chien CY, Wen TJ, Cheng YH, Tsai YT, Chiang CY, Chien CT. Diabetes upregulates oxidative stress and downregulates cardiac protection to exacerbate myocardial ischemia/reperfusion injury in rats. *Antioxidants*. 2020;9(8):679. doi:10.3390/antiox9080679

12. Zhu P, Hu S, Jin Q, et al. Ripk3 promotes ER stress-induced necroptosis in cardiac IR injury: a mechanism involving calcium overload/XO/ROS/mPTP pathway. *Redox Biol*. 2018;16:157–168. doi:10.1016/j.redox.2018.02.019

13. Gao XM, Su Y, Moore S, et al. Relaxin mitigates microvascular damage and inflammation following cardiac ischemia-reperfusion. *Basic Res Cardiol*. 2019;114(4):30. doi:10.1007/s00395-019-0739-9

14. Tomoda H, Aoki N. Coronary blood flow in evolving myocardial infarction preceded by preinfarction angina: a critical reevaluation of preconditioning effects in clinical cases. *Angiology*. 2004;55(1):9–15. doi:10.1177/000331970405500102

15. Wilde SC, Treitz C, Keppler JK, et al. β-Lactoglobulin as nanotransporter–Part II: characterization of the covalent protein modification by allicin and diallyl disulfide. *Food Chem*. 2016;197(Pt A):1022–1029. doi:10.1016/j.foodchem.2015.11.011

16. Chen X, Li H, Xu W, Huang K, Zhai B, He X. Self-assembling cyclodextrin-based nanoparticles enhance the cellular delivery of hydrophobic allicin. *J Agric Food Chem*. 2020;68(40):11144–11150. doi:10.1021/acs.jafc.0c01900

17. Li CL, Liu XH, Qiao Y, et al. Allicin alleviates inflammation of diabetic macroangiopathy via the Nrf2 and NF-kB pathway. *Eur J Pharmacol*. 2020;876:173052. doi:10.1016/j.ejphar.2020.173052

18. Mocayar Marón FJ, Camargo AB, Manucha W. Allicin pharmacology: common molecular mechanisms against neuroinflammation and cardiovascular diseases. *Life Sci*. 2020;249:117513. doi:10.1016/j.lfs.2020.117513

19. Ma LN, Li LD, Li SC, et al. Allicin improves cardiac function by protecting against apoptosis in rat model of myocardial infarction. *Chin J Integr Med*. 2017;23(8):589–597. doi:10.1007/s11655-016-2523-0

20. Ba L, Gao J, Chen Y, et al. Allicin attenuates pathological cardiac hypertrophy by inhibiting autophagy via activation of PI3K/Akt/mTOR and MAPK/ERK/mTOR signaling pathways. *Phytomedicine*. 2019;58:152765. doi:10.1016/j.phymed.2018.11.025

21. Simões SM, Rey-Rico A, Concheiro A, Alvarez-Lorenzo C. Supramolecular cyclodextrin-based drug nanocarriers. *Chem Commun*. 2015;51 (29):6275–6289. doi:10.1039/c4cc10388b

22. Soldevila-Barreda JJ, Metzler-Nolte N. Intracellular catalysis with selected metal complexes and metallic nanoparticles: advances toward the development of catalytic metallodrugs. *Chem Rev*. 2019;119(2):829–869. doi:10.1021/acs.chemrev.8b00493

23. Yan C, Liang N, Li Q, Yan P, Sun S. Biotin and arginine modified hydroxypropyl-β-cyclodextrin nanoparticles as novel drug delivery systems for paclitaxel. *Carbohydr Polym*. 2019;216:129–139. doi:10.1016/j.carbpol.2019.04.024

24. Cheng YH, He C, Riviere JE, Monteiro-Riviere NA, Lin Z. Meta-analysis of nanoparticle delivery to tumors using a physiologically based pharmacokinetic modeling and simulation approach. *ACS Nano*. 2020;14(3):3075–3095. doi:10.1021/acsnano.9b08142

25. Wang HJ, Zang J, Zhao ZH, Zhang Q, Chen SJ. The advances of neutrophil-derived effective drug delivery systems: a key review of managing tumors and inflammation. *Int J Nanomed*. 2021;16:7663–7681. doi:10.2147/IJN.S328705

26. Bejerano T, Etzion S, Elyagon S, Etzion Y, Cohen S. Nanoparticle delivery of miRNA-21 mimic to cardiac macrophages improves myocardial remodeling after myocardial infarction. *Nano Lett*. 2018;18(9):5885–5891. doi:10.1021/acs.nanolett.8b02578

27. Richart AL, Reddy M, Khalaji M, et al. Apo AI nanoparticles delivered post myocardial infarction moderate inflammation. *Circ Res*. 2020;127 (11):1422–1436. doi:10.1161/circresaha.120.316848

28. Li Z, Hu S, Huang K, Su T, Cores J, Cheng K. Targeted anti-IL-1β platelet microparticles for cardiac detoxing and repair. *Sci Adv*. 2020;6(6): eaay0589. doi:10.1126/sciadv.aay0589

29. Zhang Q, Dehaini D, Zhang Y, et al. Neutrophil membrane-coated nanoparticles inhibit synovial inflammation and alleviate joint damage in inflammatory arthritis. *Nat Nanotechnol*. 2018;13(12):1182–1190. doi:10.1038/s41565-018-0254-4

30. Wu M, Zhang H, Tie C, et al. MR imaging tracking of inflammation-activatable engineered neutrophils for targeted therapy of surgically treated glioma. *Nat Commun*. 2018;9(1):4777. doi:10.1038/s41467-018-07250-6

31. Song Y, Kadiyala U, Weerappuli P, et al. Antimicrobial microwebs of DNA-histone inspired from neutrophil extracellular traps. *Adv Mater*. 2019;31(14):e1807436. doi:10.1002/adma.201807436

32. Zhang C, Zhang L, Wu W, et al. Artificial super neutrophils for inflammation targeting and HClO generation against tumors and infections. *Adv Mater*. 2019;31(19):e1901179. doi:10.1002/adma.201901179

33. Shi P, Cao Y, Gao J, et al. Allicin improves the function of cardiac microvascular endothelial cells by increasing PECAM-1 in rats with cardiac hypertrophy. *Phytomedicine*. 2018;51:241–254. doi:10.1016/j.phymed.2018.10.021

34. Bai J, Wang Q, Qi J, et al. Promoting effect of baicalin on nitric oxide production in CMECs via activating the PI3K-AKT-eNOS pathway attenuates myocardial ischemia-reperfusion injury. *Phytomedicine*. 2019;63:153035. doi:10.1016/j.phymed.2019.153035

35. Liu XM, Yang ZM, Liu XK. Fas/FasL induces myocardial cell apoptosis in myocardial ischemia-reperfusion rat model. *Eur Rev Med Pharmacol Sci*. 2017;21(12):2913–2918.

36. Costantino S, Akhmedov A, Melina G, et al. Obesity-induced activation of JunD promotes myocardial lipid accumulation and metabolic cardiomyopathy. *Eur Heart J*. 2019;40(12):997–1008. doi:10.1093/eurheartj/ehy903

37. Zhou H, Li D, Zhu P, et al. Inhibitory effect of melatonin on necroptosis via repressing the Ripk3-PGAM5-CypD-mPTP pathway attenuates cardiac microvascular ischemia-reperfusion injury. *J Pineal Res*. 2018;65(3):e12503. doi:10.1111/jpi.12503

38. Zhou H, Wang J, Zhu P, Hu S, Ren J. Ripk3 regulates cardiac microvascular reperfusion injury: the role of IP3R-dependent calcium overload, XO-mediated oxidative stress and F-action/filopodia-based cellular migration. *Cell Signal*. 2018;45:12–22. doi:10.1016/j.cellsig.2018.01.020

39. Ma S, Sun L, Wu W, Wu J, Sun Z, Ren J. USP22 protects against myocardial ischemia-reperfusion injury via the SIRT1-p53/SLC7A11-dependent inhibition of ferroptosis-induced cardiomyocyte death. *Front Physiol.* 2020;11:551318. doi:10.3389/fphys.2020.551318

40. Stamenkovic A, O'Hara KA, Nelson DC, et al. Oxidized phosphatidylcholines trigger ferroptosis in cardiomyocytes during ischemia-reperfusion injury. *Am J Physiol Heart Circ Physiol.* 2021;320(3):H1170–h1184. doi:10.1152/ajpheart.00237.2020

41. Yamada N, Karasawa T, Wakiya T, et al. Iron overload as a risk factor for hepatic ischemia-reperfusion injury in liver transplantation: potential role of ferroptosis. *Am J Transplant.* 2020;20(6):1606–1618. doi:10.1111/ajt.15773

42. Zhou J, Li YS, Chien S. Shear stress-initiated signaling and its regulation of endothelial function. *Arterioscler Thromb Vasc Biol.* 2014;34 (10):2191–2198. doi:10.1161/atvbaha.114.303422